


Fluid injection-induced fracture activation and damage evolution in naturally fractured reservoirs

Other Conference Item**Author(s):**

[Lei, Qinghua](#) ; Gholizadeh Doonechaly, Nima; Tsang, Chin-Fu

Publication date:

2020-11

Permanent link:

<https://doi.org/10.3929/ethz-b-000454682>

Rights / license:

[In Copyright - Non-Commercial Use Permitted](#)

Fluid injection-induced fracture activation and damage evolution in naturally fractured reservoirs

Qinghua Lei^{1,*}, Nima Gholizadeh Doonechaly¹, Chin-Fu Tsang^{2,3})

1) Department of Earth Sciences, ETH Zürich, Zürich, Switzerland

2) Department of Earth Sciences, Uppsala University, Uppsala, Sweden

3) Energy Geosciences Division, Lawrence Berkeley National Laboratory, Berkeley, USA

*Corresponding author: qinghua.lei@erdw.ethz.ch

1. Introduction

Injection of large-volume fluid into subsurface rocks at considerable depths has been carried out in many geoenvironmental applications such as geothermal energy and oil/gas recovery. One of the main purposes of fluid injection in these projects is to stimulate a geological formation to gain improved connectivity of fracture systems and increased productivity of heat/hydrocarbon resources. Nevertheless, such a hydraulic stimulation treatment often causes the activation of natural fractures (e.g. critically stressed faults) and produce man-made earthquakes, which provoke significant societal concerns (Ellsworth, 2013). Thus, it is of central importance to understand the multiphysical processes undergoing in deep reservoirs during fluid injection in order to better optimise the stimulation strategy, while minimising seismicity risk. In this research, we develop a new numerical model aiming to achieve a full coupling of hydro-mechanical processes in fractured porous rocks and apply the model to study fluid injection-triggered responses in naturally fractured rocks. We demonstrate that our model is an effective tool for unravelling the important role of natural fracture networks in hydraulic stimulation of geological media.

2. A fully-coupled hydro-mechanical model

The mechanical equilibrium of a fractured porous rock is governed by:

$$\nabla \cdot \boldsymbol{\sigma} + \mathbf{f} = 0, \quad (1)$$

where $\boldsymbol{\sigma}$ is the stress and \mathbf{f} is the body force. The stress-strain relation obeys linear poro-elasticity incorporating an isotropic damage law (Jirásek and Bauer, 2012):

$$\boldsymbol{\sigma}' = \boldsymbol{\sigma} - \alpha p \mathbf{I} = (1 - \omega) \mathbf{D} : \boldsymbol{\varepsilon}, \quad (2)$$

where $\boldsymbol{\sigma}'$ is the effective stress, α is the Biot's coefficient, p is the fluid pressure, ω is the scalar damage parameter, \mathbf{I} is the identity matrix, \mathbf{D} is the elastic stiffness matrix, and $\boldsymbol{\varepsilon}$ is the strain.

The isotropic damage model is used aiming to mimic failure processes in rock materials, which are governed by the loading-unloading conditions as (Jirásek and Bauer, 2012):

$$f(\tilde{\boldsymbol{\varepsilon}}, \kappa) \leq 0, \quad \dot{\kappa} \geq 0, \quad \dot{\kappa} f(\tilde{\boldsymbol{\varepsilon}}, \kappa) = 0, \quad (3)$$

where $\tilde{\boldsymbol{\varepsilon}}$ is the equivalent strain, and κ is an internal variable. We define the equivalent tensile and compressive strains (Jirásek and Bauer, 2012) as:

$$\tilde{\boldsymbol{\varepsilon}}_t = -\frac{\| \langle -\mathbf{D} : \boldsymbol{\varepsilon} \rangle \|}{E}, \quad \tilde{\boldsymbol{\varepsilon}}_c = \frac{\| \langle \mathbf{D} : \boldsymbol{\varepsilon} \rangle \|}{E}, \quad (4)$$

where $\|\cdot\|$ is the norm operator, $\langle \cdot \rangle$ are the Macaulay brackets denoting the positive part and E is the Young's modulus. The tensile and compressive damage parameters, ω_t and ω_c , are then derived by assuming an elasto-brittle constitutive behaviour (Tang et al., 2008):

$$\omega_t = \begin{cases} 0, & \kappa_t \geq \varepsilon_{t0} \\ 1 - \frac{f_{tr}}{E\kappa_t}, & \kappa_t < \varepsilon_{t0} \end{cases}, \quad \omega_c = \begin{cases} 0, & \kappa_c \leq \varepsilon_{c0} \\ 1 - \frac{f_{cr}}{E\kappa_t}, & \kappa_c > \varepsilon_{c0} \end{cases}, \quad (5)$$

where $\varepsilon_{t0} = f_{t0}/E$ and $\varepsilon_{c0} = f_{c0}/E$ are the limit elastic tensile and compressive strains, respectively; f_{t0} and f_{c0} are the tensile and compressive strengths, respectively; $f_{tr} = \eta f_{t0}$ and $f_{cr} = \eta f_{c0}$ are the residual tensile and compressive strengths, respectively, with η being the residual strength ratio.

The aperture of a fracture under normal compression may follow (Rutqvist et al., 2002):

$$b_n = b_r + (b_0 - b_r) \exp(-\xi \sigma'_n), \quad (6)$$

where b_n is the normal aperture, b_0 is the initial aperture, b_r is the residual aperture, $\sigma'_n = \sigma_n - p$ is the effective normal compressive stress with σ_n being the total normal stress and p the fluid pressure, and ξ is the stress-aperture correlation coefficient that equals to $1/[K_{n0}(b_0 - b_r)]$ with K_{n0} being the initial normal stiffness. The normal stiffness of the fracture under compression is:

$$K_n = -\frac{\partial \sigma'_n}{\partial b_n} = \frac{b_0 - b_r}{b_n - b_r} K_{n0}, \quad (7)$$

The shear behaviour of a rock fracture is based on Coulomb's friction law as:

$$\tau_s = \begin{cases} K_s u_s, & u_s < u_p, \\ \tau_p, & u_s \geq u_p \end{cases}, \quad (8)$$

where τ_s is the shear stress, u_s is the shear displacement, K_s is the fracture shear stiffness, $\tau_p = \sigma'_n \tan \varphi_f$ is the peak shear stress, φ_f is the friction angle, and $u_p = \tau_p / K_s$ is the peak shear displacement beyond which the fracture starts to slide. The shear-induced dilation is related to the shear displacement via an incremental formulation as:

$$dv_s = \begin{cases} -\tan \varphi_d du_s, & u_p \leq u_s \leq u_r, \\ 0, & \text{else} \end{cases}, \quad (9)$$

where φ_d is the dilation angle, and u_r is the residual shear displacement. The fracture aperture b_f under combined normal and shear deformation is then given as:

$$b_f = b_n - v_s. \quad (10)$$

Fluid flow is governed by the continuity and momentum equations, which may reduce to:

$$\rho_w \left(S \frac{\partial p}{\partial t} + \alpha \frac{\partial \varepsilon_v}{\partial t} \right) - \nabla \cdot \left(\frac{\rho_w k}{\mu_w} \nabla p \right) = Q. \quad (11)$$

where ρ_w and μ_w are the density and dynamic viscosity of water, ϕ is the porosity, k is the permeability, t is the time, Q is the source term, and ε_v is the volumetric strain of the solid skeleton. For natural fractures, the permeability is related to the fracture aperture based on the cubic law as $k_f = b_f^2 / 12$; the storage coefficient is calculated as $S_f = c_w + 1 / (K_n b_f)$, where c_w is the compressibility of water. It is assumed that there is no infilling material in natural fractures and therefore $\phi_f = 1$. For rock matrix, the porosity ϕ_m is derived as (Rutqvist et al., 2002): $\phi_m = \phi_r + (\phi_0 - \phi_r) \exp(-\zeta \sigma'_m)$, where ϕ_0 is the initial porosity, ϕ_r is the residual porosity, σ'_m is the effective mean stress, and ζ is the porosity-stress correlation coefficient that is substituted by $c_m / (\phi_0 - \phi_r)$ for undamaged rock ($\omega = 0$) and $1 / [K_n (b_0 - b_r)]$ for damaged rock ($\omega > 0$). The permeability of rock matrix is then given as (Zhu and Wei, 2011): $k_m = k_0 (\phi_m / \phi_0)^3 \exp(\zeta \omega)$, where k_0 is the initial matrix permeability and ζ is the damage-permeability correlation coefficient estimated as $\ln[b_0^3 / (12k_0h)]$ with h being the local element size. The storage coefficient of the rock matrix is given as (Rutqvist et al., 1998): $S_m = \phi_m c_w + (1 - \alpha)(\alpha - \phi_m)c_m$, where $c_m = 3(1 - 2\nu) / E$ is the drained compressibility of the rock matrix.

3. Model setup and simulation results

We consider hypothetically a 2D square fractured rock domain (horizontally placed) of size $L = 100$ m, located at a depth of 3600 m in granitic rock. The out-of-plane thickness is assumed to be 20 m. The rock domain is embedded with a network of 100 natural fractures belonging to two systematic sets oriented at 30° and 120° with respect to the positive x direction. The spatial location of fractures is purely random. The fractures are assumed to have a constant length $l = 15$ m or 27 m, rendering a network with a dimensionless fracture density $\chi = \sum (l_i/2)^2 / L^2 = 0.5$ or 1.5 , respectively. The generated low ($\chi = 0.5$) and high ($\chi = 1.5$) density fracture networks are on the two sides of the percolation threshold ($\chi_c \approx 1.0$). The rock domain is subject to a stress state with the maximum horizontal stress $S_H = 90$ MPa and the minimum horizontal stress $S_h = 46$ MPa, imposed orthogonally to the domain along the x and y directions, respectively. The initial pore fluid pressure is $p_0 = 31$ MPa. The material properties of rock matrix, natural fractures and water in general resemble those of the Fenton Hill test site (Norbeck et al., 2018). To stimulate the rock mass, water is injected at a constant rate of 1×10^{-4} m²/s for up to 1 hr with

the injection point located at the domain centre, which also coincides with the centre of a pre-existing fracture.

Fig. 1a shows the spatial and temporal evolution of damage and pressure and stress in the fractured rocks with $\chi = 0.5$ during fluid injection. At the beginning ($t = 0$ hr), the system is in its initial equilibrium state, where the pressure field is homogeneous. When water starts to be injected into the fractured rock ($t = 0.25$ hr), fluid pressure quickly builds up in the fractures that originally connect to the injection point. The elevated pore fluid pressure then activates some of these natural fractures such that wing cracks emanate from their tips and propagate in general along the direction of the maximum principal stress, i.e. x direction. Only small amount of water diffuses into the matrix due to its low permeability and that the high pressure mainly concentrates in the locally connected fracture cluster. Some low pressure appears in the matrix a few metres away from activated fractures, attributed to the poro-elastic effect. As more water is injected into the system ($t = 0.5$ hr), wing cracks continue to propagate and eventually link with other fractures that are originally not connected to the injection point. Those fractures also start to accommodate high fluid pressure and finally serve as the pathways for the water to migrate out of the domain ($t = 0.75$ hr). It seems that when a percolated pathway is able to link the injection point to the domain boundary, no new damage would emerge ($t = 0.75$ -1 hr).

We then analyse the spatial and temporal evolution of damage and pressure in the rock domain with $\chi = 1.5$ (Fig. 1b). In this case, similarly at the beginning ($t = 0$ hr), the pressure field is very uniform. When water is injected into the fractured rock ($t = 0.25$ hr), high fluid pressure first builds up along interconnected fractures close to the injection point. As more water is injected ($t = 0.5$ -1 hr), a progressively larger cluster of fractures is occupied by high pressure fluid. However, such a cluster is mainly formed by pre-existing fractures, and only minor new damage emerges in the system. It is noted that although most fractures in this high-density fracture network can find a connected path to link them with the injection point, only some of them are activated to accommodate high fluid pressure.

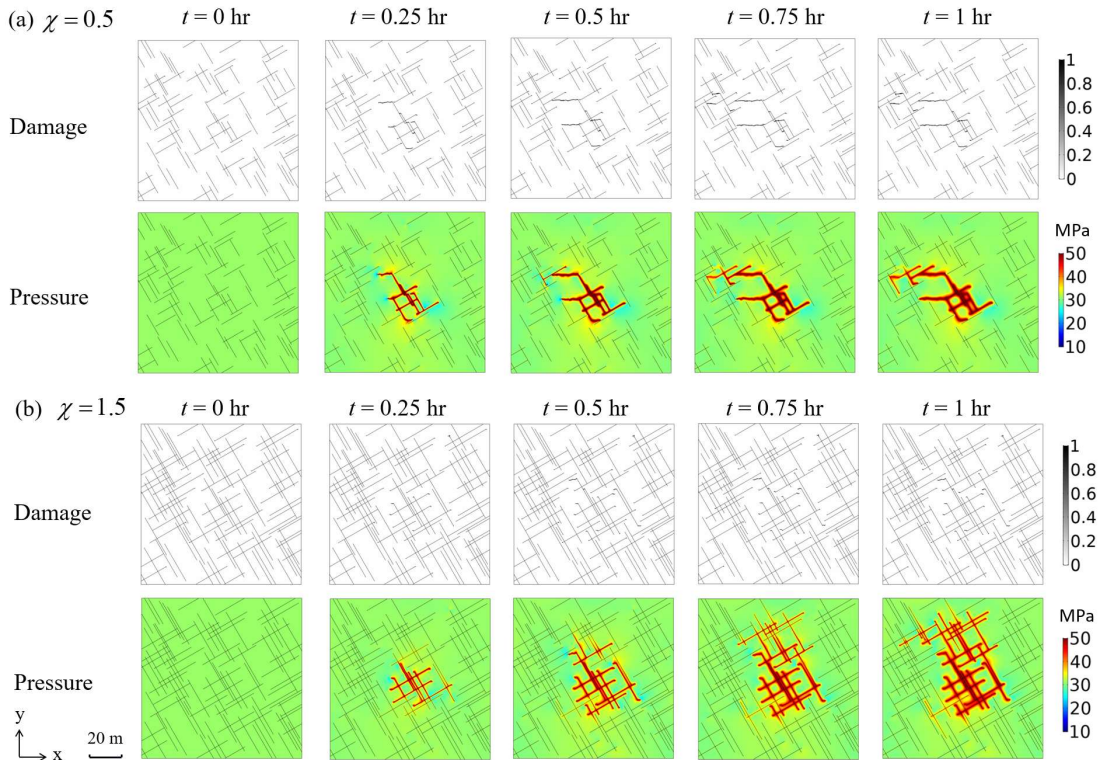


Fig. 1. Damage propagation and pressure evolution in the fractured rock with a fracture density of $\chi =$ (a) 0.5 and (b) 1.5 during fluid injection.

In Fig. 2, we show the shear displacement of pre-existing fractures before and after the hydraulic stimulation as well as the changes. Prior to fluid injection, in both networks, the

fractures of the set oriented at 30° with respect to the x direction are highly sheared due to their preferential orientation for shearing under the given far-field stress state. After the stimulation, some fractures belonging to the 120° set experience significant shear dislocation under the elevated pore pressure, which further promotes shear dilation and aperture enlargement allowing more water to flow through them. Such a positive feedback operates until a hydraulically connected pathway (i.e. backbone) is eventually formed and/or activated linking from the injection point to the domain boundary. Clearly, more pre-existing fractures are activated for shearing in the high density fracture network. In both networks, the 120° set, which is less sheared in the natural state, is more activated for shearing and dilating by the injection. This is because fluid has to open these fractures that form critical pathways in order to migrate through them to reach larger areas, whereas fractures of the 30° set are already associated with quite large apertures before stimulation and thus can in general support the flow.

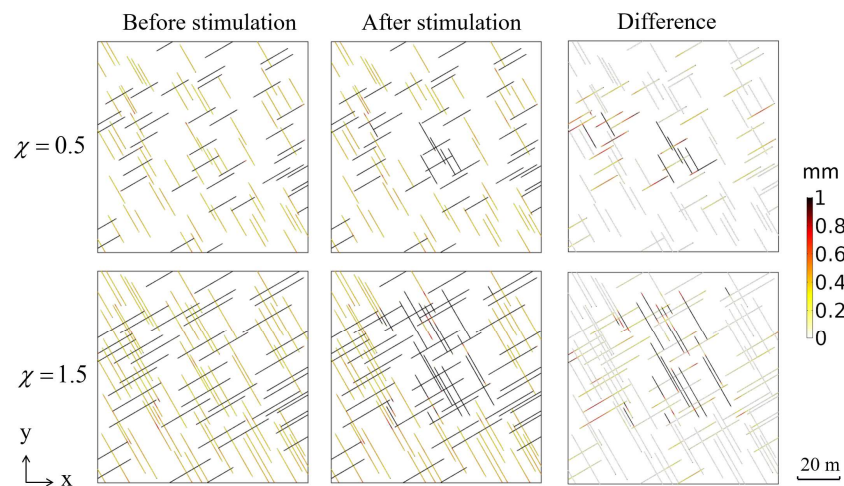


Fig. 2. Shear displacement of pre-existing fractures in the fractured rock before (left panel) and after (middle panel) the stimulation as well as the changes (right panel).

To sum up, in this research, we developed a fully-coupled hydro-mechanical model to simulate fluid injection-induced activation of pre-existing fractures and propagation of new damages in naturally fractured rocks. In our simulation, we observe a strong control of natural fracture network connectivity on the damage emergence and shear reactivation in rock masses. The results of our research have important implications for injection-related engineering activities.

References

- Ellsworth WL. 2013. Injection-induced earthquakes. *Science* 341, 1225942–1225942.
- Jirásek M, Bauer M. 2012. Numerical aspects of the crack band approach. *Computers & Structures* 110–111, 60–78.
- Norbeck JH, McClure MW, Horne RN. 2018. Field observations at the Fenton Hill enhanced geothermal system test site support mixed-mechanism stimulation. *Geothermics* 74, 135–149.
- Rutqvist J, Noorishad J, Tsang C-F, Stephansson O. 1998. Determination of fracture storativity in hard rocks using high-pressure injection testing. *Water Resources Research* 34, 2551–2560.
- Rutqvist J, Wu Y-S, Tsang C-F, Bodvarsson G. 2002. A modeling approach for analysis of coupled multiphase fluid flow, heat transfer, and deformation in fractured porous rock. *International Journal of Rock Mechanics and Mining Sciences* 39, 429–442.
- Tang CA, Liang ZZ, Zhang YB, Chang X, Tao X, Wang DG, Zhang JX, Liu JS, Zhu WC, Elsworth D. 2008. Fracture spacing in layered materials: A new explanation based on two-dimensional failure process modeling. *American Journal of Science* 308, 49–72.
- Zhu WC, Wei CH. 2011. Numerical simulation on mining-induced water inrushes related to geologic structures using a damage-based hydromechanical model. *Environmental Earth Sciences* 62, 43–54.